Conference Paper, Published Version

Pinel, Sebastien; Bonnet, Marie-Paule; Da Silva, Joecila S.; Catry, Thibault; Seyler, Frederique

Flooding dynamics within an Amazonian floodplain: water circulation patterns and inundation duration

Zur Verfügung gestellt in Kooperation mit/Provided in Cooperation with:
TELEMAC-MASCARET Core Group

Flooding dynamics within an Amazonian floodplain: water circulation patterns and inundation duration

Sebastien Pinel[1], Marie-Paule Bonnet[2], Joecila S. Da Silva[1], Thibault Catry[2], Frederique Seyler[2]

[1] RHASA
Amazon state University (UEA)
Manaus, Brazil
sebpinel@gmail.com; jsdsilva@uea.edu.br;

[2] UMR 228 Espace-DEV Research Institute for Development (IRD)
Montpellier, France
marie-paule.bonnet@ird.fr; thibault.catry@ird.fr

Abstract—**Amazonian floodplains ensure fundamental hydro-ecological functions and support a high level of biodiversity. Transformation in the Amazon basin, land use changes, dam construction and climate variability, increasingly threaten these emblematic ecosystems. In view of supporting their conservation, it is important to monitor the spatiotemporal distribution of key variables such as flood extent, inundation duration, and water velocities that constrain species habitats. However, floodplains are scarcely surveyed, and hydrological information is commonly restricted to water level and discharge measured in the mainstream. As a solution, 2D-hydrodynamics modelling allows monitoring these threatened zones and getting new information such as water circulation. Flooding dynamics across a medium-size floodplain system (Janauacá Lake, 786 km^2) along the Amazon/Solimões River over a 9-years period (2006–2015) is studied through integration of remote sensing and limited *in situ* data in hydrologic-hydrodynamic modelling based on Telemac-2D model. We firstly detail the methodological approach and the modelling assessment in terms of water level, flood extent and velocity. It correctly reproduces floodplain water level (Nash-Sutcliffe Efficiency=0.97) and flood extent (averaged Threat Score=62) and horizontal velocity (Nash-Sutcliffe Efficiency >0.68). The model's high accuracy varies along the hydrological year. Then, we focused on seasonal and inter-annual spatial variability of water circulation and inundation duration. We highlighted strong heterogeneities in water velocity magnitude between the different morphological domains of the floodplain, the highest velocities being encountered in the river-floodplain channel. In addition to topography, we emphasized the importance of the mainstream and the local runoff in controlling the water circulation, at least during part of the hydrological year. During the early rising period, local runoff constrains the river incursion across the floodplain, while the rates of mainstream rising/receding controls the flood duration. The comparison of several hydrological years highlights the interannual changes of these hydraulic controls and also the influence exerted by prior inundation conditions. While we observed only few changes in water velocity distribution among hydrological years, the inundation duration is highly variable. Extreme flood events may induce positive (up to 40 days) but also negative (up to -20 days) anomalies of inundation duration.**

I. Introduction

Wetlands and floodplains (FP) cover about 14% of the Amazon Basin. In the lowland Amazon, FPs roughly occupy 800,000 km^2 [1]. They trap substantial amounts of sediment [2]. High primary production in FPs partly supplies the mainstream with labile organic matter [3] and regulates CO2 or CH4 emissions [4]. They are essential components regulating flow propagation [5]. They support fisheries yields [6] and host several endangered species [7]. In coming years, FPs will be increasingly threatened by in-river infrastructure [8]. Conjointly with climate change, these expected development trends seriously endanger Amazon FP ecosystems and biodiversity [9].

Large seasonal variations of water level and highly smooth topography generate complex inundation patterns. Water quality and habitats characteristics are tightly related with FP water circulation. Flood amplitude and water velocity across the FP drive the inundation extent and key-variables such as depth, habitat connectivity and hydroperiod that control suspended and dissolved material fates and species distribution and interactions [10]. As shown by local hydrological studies, in-waters originate from the mainstream and from local sources such as hyporheic water, local runoff and direct precipitation [11]. The mixing area between these water sources, its extent and location through the FP depend on water head distribution within the different ponds and significantly vary along the corridor and hydrological year.

Full 2D hydrodynamics models appear to be a good tool to study FP. However, they present the inconvenient to be time-consuming. The LISFLOOD-FP hybrid model [12] based on simplified propagation equations appears as a solution for modelling studies over Amazon FP. Based on this hybrid model or on simple flow routing schemes. Several modelling studies have focused on FP hydrology: at regional scale [13], medium scale [14], and local scale in the lowland Amazon [11]. These studies essentially focused on capturing flood extents (FE), water level, exchanged fluxes with the mainstream and stored water volume throughout HY. Only few studies involved a full 2D hydrodynamics model in the Amazon FPs that allow accurate velocity modelling. References [15,16] coupled a sedimentation module to a hydrodynamics model to study the planform dynamics of anabranching structures. Finally, in the Amazon, water circulation across the FP have been little investigated. References [17,18] presented the most comprehensive studies of water head distribution within a lowland Amazon FP but did not specifically address velocity patterns across the FP.

In this study, we combine *in situ* information, remote sensing and a hydrologic-hydrodynamic modelling to simulate

flooding dynamic in a medium-size Amazonian FP and investigate spatial velocity patterns and flood frequency. We firstly present i) the methodology and the necessary datasets; ii) the hydrologic-hydrodynamic model performance in reproducing water level, flood extent and velocity. Then we employed this model to i) exhibit spatial velocity patterns and flood frequency at seasonal scale, ii) examine the influence of extreme drought or flood events on velocity patterns and flood duration.

II.   STUDY ZONE

The study site is the Janauacá FP (3.200°S-3.250°S, 60.230°W-60.130°W, Amazon state, Brazil), a medium-size FP located on the right bank of the Amazon/Solimões River, 40 km upstream its junction with the Negro River. It is formed by the mixture of a várzea (the North-east part) and a ria-lake, a composition rather typical along this Amazon/Solimões River reach. The mainstream at this location generally exhibits a monomodal flood phase, rising regularly from November to June. The Amazon/Solimões River is commonly considered as a "white-water" river [19]. The Janauacá FP is composed of a lake with fringing wetlands and inundated forest, linked to the mainstream by a unique channel (Figure 1a-b). The FP and its local drainage basin extend over 786 km² (Pinel et al., 2015). Flood extent seasonally varies from 4% to 50% of the FP watershed, with water level variations between 10 m and 24 m. Like other Amazon FPs, flooding is ensured by several water sources: mainstream through channelized flow or overflow that is the main source but and local runoff, hyporheic water and direct rainfall. From late low water period to mid rising period, the channel acts as an inlet until overflow starts. The mainstream water quality highly contrasts with water quality of small tributaries that is closer to "black water" properties.

III.   MATERIAL AND METHODS

A. Modelling approach and settings

The modelling approach relies on the coupling of two models: a hydrological model, which simulate runoff from the uplands, followed by a hydrodynamics model.

The hydrological model LUMP-FP, developed and applied to the study site [11], was used to produce runoff from the upland local watershed as boundary condition for the hydrodynamic model (Figure 1b). We used the same settings as [11] to generate daily runoff for the study period extending from 11/01/2006 to 12/31/2015.

The TELEMAC-MASCARET system is freely available at www.opentelemac.org and was designed for computational fluid dynamics [20]. We specifically used its two dimensional (2D) hydrodynamic module (TELEMAC-2D v7p3) that simulates free-surface flows in the two dimensions of horizontal space. For more details, readers are referred to the TELEMAC-2D user manual [21].

The modelled domain was limited to the pixels whose elevation was lower than 29 m, i.e. the domain that contains the floodable area (Figure 1b). The initial pixels water level condition was set to the RL1 value at the 11/01/2006, and velocity was assumed null in the whole domain. The hydrodynamic model requires boundary conditions: i) water flow boundary condition (inflow from the local basins); ii) water level boundary conditions (WLBC) (inflow from the mainstream) in which observed mainstream stage is imposed.

LUMP-FP model provided the total discharge from the uplands. Based on sub-catchment area ratio, we distributed the flow among the different streams draining the local watershed. Regarding WLBC, the combination of visual inspection of ALOS-1/PALSAR images and mainstream stage allowed
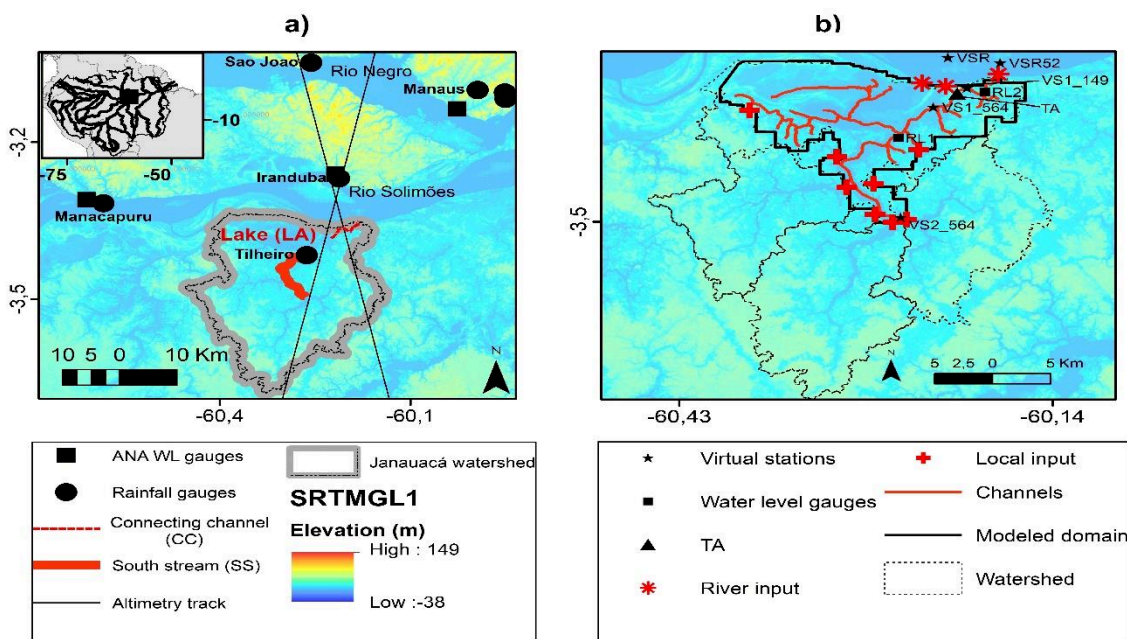

Figure 1. a) Study site with the locations of available water level and rainfall gauges, b) Model domain with background SRTMGL1 and boundaries location

determining the zones associated with overflow and corresponding water level thresholds. We identified: WLBC1 (water level boundary condition 1) underwater for a water level of 19.50 m at 49 km downstream Manacapurú, and WLBC2 underwater for a level of 20.00 m at 47 km downstream Manacapurú (Figure 1b). At these locations, we modified the levee elevations to match these elevation thresholds. At last, the junction between the mainstream and the connecting channel constitutes the third WLBC3. Water level at these three boundary conditions were linearly derived from the VSR gauge (VSR47, VSR49 and VSR52).

TELEMAC-2D model offers several options for calculation. Here, we chose the method of characteristics to simulate velocity advection and the propagation step is solved by the conjugate gradient method with a diagonal preconditioning which ensures numerical stability. We used a constant viscosity set to 10-6 m².s^{-1} and a constant water density set to 996.1 kg.m^{-3} [22]. Bottom friction was based on the Manning coefficient map. We used the Blue Kenue software [23] to generate a mesh of 224 527 triangular elements with sides ranging from 23 m to 77 m. The model was run from 11/01/2006 to 12/31/2015 using a 30 s time-step on a multi-core cluster environment: the Altix-XE 340 cluster platform, located at LNCC (*Laboratório Nacional de Computação Científica*, Brazil).

B. Calibration and validation assessment

As LUMP-FP model was fully validated for the study site [11], and as we used same settings and the same simulation period, further calibration and validation were not necessary for this model. However, we calibrated the hydrodynamic model (TELEMAC component) against water level measured at RL1 and RL2 from April 2007 (rising water) to January 2008 (low water) adjusting Manning coefficients by a trial-and-error method. The model was validated in terms of vertical, horizontal and velocity accuracy. The reference datasets for the vertical validation were water level measured at RL1, RL2, VS1_564, VS2_564, and VS1_149. The horizontal validation consisted in comparing modelled and ALOS-1/PALSAR-deduced flood extents. Velocity accuracy was controlled against *in situ* measurements.

Several classical statistics served to appraise model vertical accuracy: the Pearson correlation coefficient, the RMSE (m), the Nash-Sutcliffe efficiency (NSE). The horizontal accuracy was assessed using the following skills scores: the Threat Score (TS) measures the model accuracy with a perfect score of 100; the bias index (BIAS) indicates the type of error (overestimation or underestimation). Those scores are determined using the following relations: $TS=100(a/(a+b+c))$; $BIAS=100(1-(a+b)/(a+c))$; where, a is the area that is both mapped and modelled as inundated, b is the inundated area modelled but not mapped, and c is the inundated area mapped but not modelled.

C. Available datasets and consolidation towards modelling

Water level time series

Daily stages data from two gauges of the Brazilian national network, namely Manacapurú gauge (3.317°S, 60.583°W) and Iranduba gauge (3.268°S, 60.215°W) were retrieved from the Brazilian water agency (ANA) website. Two additional gauges were installed in the Janauacá FP at "RL1" (3.424°S, 60.264°W) and "RL2" (3.368°S, 60.193°W) (Figure 1b). All the gauges were levelled by a high-precision bi-frequency Global Positioning System (GPS) unit.

We also used water level data from altimetry satellites: the ENVISAT/RA-2 altimeter operated by European Spatial Agency (2002-2010) and its follow-on French-Indian joint mission SARAL/ALtiKa altimeter in operation on the same orbit since 2013. Both furnish reliable measurements every 35 days [24]. We produced 7 virtual stations (VS) (Figure 1b): VS1_564, VS2_564, VS1_149, VSR_149 and VSR_564 in the FP, and VSR_564 and VSR_149 in the mainstream. The two latter being close (1.6 km), we merged both into a unique station denoted VSR hereafter. We used a linear relationship between Manacapurú gauge and VSR water level to produce daily mainstream stages at VSR52 (located 52 km downstream from Manacapurú)

Rainfall and meteorological data

We used daily rainfall data from six gauges from the Brazilian national network, downloaded from the ANA website (Figure 1a). Averaged rainfall on the FP was obtained weighting each gauge data series by the Thiessen polygon area. The Brazilian national meteorological institute (INMET) provided hourly climatic data from the nearest meteorological station (Manacapurú, Brazil, Para state, 3.317°S, 60.583°W) through its website. We used the following meteorological parameters: insolation (W.m^{-2}), wind speed (m.s^{-1}), wind direction, air relative humidity (%), air temperature (°C) and pressure (hPa) useful for evapotranspiration computation in the hydrological modelling step.

Bottom friction map

We used the dual–season wetlands map of Amazon Basin [25] to define zones with same cover assumed to reflect friction properties in the FP. This product is available at the NASA Earth Observing System Data and Information System (EOSDIS) website. From this classification map, we retained 4 distinct classes: permanent water, shrubs, flooded forest and forest in spatial proportions of 44%, 14%, 21%, and 20%, respectively. The Manning coefficient attributed to each zone follows literature advises [26]: 0.02-0.04, 0.03-0.06, 0.05-0.15 and 0.1-0.2 for permanent water, shrubs, flooded forest, and forest, respectively. Adjusting the Manning coefficient is part of the hydrodynamic model calibration step.

Topography and bathymetry data

We used the topography dataset produced by [27] for the study area. This dataset was derived from SRTMGL1 (30 m-resolution) dataset. Combining *in situ* bathymetry and remotely sensed products, these authors removed the interferometric bias and the vegetation-induced bias. Then, they interpolated the unbiased elevations, the bathymetric data using the ANUDEM v5.3 algorithm [28] constrained by a drainage channel network. The produced topographic map presents a vertical accuracy of 1.7 m for a 30 m resolution [27]. Moreover, the method proposed by [27] ensures numerical stability of the mesh processing and the hydrodynamics model.

Flood extent from ALOS/PALSAR imagery

Due to limitations in retrieving water under forest, product based on optical imagery were not adapted to this study. As an alternative, L-band Synthetic Aperture RADAR (SAR) permits this detection. We performed a thresholding classification based on ALOS-1/PALSAR images, available through the ALOS Kyoto & Carbon initiative at the Alaska Satellite Facility website. We retrieved 24 scenes covering the whole range of water level conditions to better capture the flood pulse dynamics.

Velocity data

Averaged velocities of cross-sections were measured with an Acoustic Doppler Current Profiler (ADCP) (RDI instrument 1200 Hz) at the Terra Alta (TA) location ($3.370°S$, $60.214°W$) and RL2 gauge location (Figure 1b). These two locations permitted measuring the channel discharges within a short distance from RL2 gauge. At last, the velocity dataset consisted of 30 measures collected during the 2006-2011 period.

Water circulation pattern analysis

To examine seasonal velocity patterns, we partitioned both space and time. An hydrological year was subdivide into six hydrologic periods: i) late low water, ii) early rising water, iii) late rising water, iv) high water, v) falling water, vi) early low water. All hydrologic periods were defined from RL1 stages time-series.

Also, the FP was subdivided into three distinct domains: the lake area with fringing flooded forests and other wetlands (denoted LA, hereafter) from the south stream (denoted SS, hereafter) as suggested by these authors, and, we extended this partition to include the connecting channel (denoted CC, hereafter) (Figure 1a). By convention, positive velocities and slopes indicate water flowing from river to FP.

To examine spatial inundation frequency, for each mesh node and each hydrological year, we computed the inundation duration, i.e. the number of days during which a node is flooded. The inundation frequency map was deduced from the average of the duration of inundation of each node over each simulated hydrological year and reported to the length of the longest hydrological year over the study period.

The study period encompasses one extreme drought during 2009-2010 hydrological year and several extreme floods (2008-2009, 2011-2012 and 2014-2015 hydrological years). We computed the difference in inundation duration between the normal year and the extreme drought or flood hydrological years to build anomaly maps of inundation duration.

IV. RESULTS

A. Model performance assessment

Water level

It is noteworthy to mention that the hydrodynamic model was poorly sensitive to the choice of the Manning parameter: the averaged RMSE varied from 0.37 m to 0.41 m when exploring the whole range of Manning values. We finally selected the values giving the lowest RMSE: 0.032, 0.042,

0.14 and 0.18 $s.m^{-2/3}$ for permanent water, shrubs, flooded forest, and forest zones, respectively.

The simulated and observed water level are in good agreement at all gauges. Global RMSE, NSE and correlation coefficient at the fifth stations over the entire period were 0.32 m, 0.99 and 0.99, respectively. Comparing to the accuracy of the bathymetry (1.70 m) and the amplitude of the flood wave (11.05 m), the RMSE value remained low. The validation upon VS (RMSE, NSE and correlation coefficient of 0.30 m, 0.99 and 0.99, respectively) remained similar to the ones upon *in situ* gauges (RMSE, NSE and correlation coefficient of 0.38 m, 0.99, and 0.99, respectively). The vertical accuracy also has temporal variations. RMSE, NSE and correlation coefficient presented the lowest values at low water with scores of 0.48 m, 0.75, and 0.93, respectively. Best scores are obtained during rising water (RMSE, NSE and correlation coefficient of 0.17 m, 0.99 and 0.99, respectively).

Flood extent

The overall horizontal accuracy TS was 62 (Table 1). The averaged positive BIAS (20) suggested a slight flood extent under-prediction by the model. Nevertheless, the discrepancies magnitude showed temporal variations depending on the FP stage. For water level > 15 m, i.e. during rising water, high water and early falling water, skills scores remained good (TS>58). Positive BIAS (22-38) render a slight model underestimation. Conversely, for water level <15 m, the skills scores testify for a model overestimation (negative BIAS) with a lower accuracy (TS<48). This analysis also evidences geomorphological controls that confine inundation and critical thresholds (12 m, 15 m and 21 m). Indeed, for very low water level, the inundation remains confined to the inner drainage channels and small ponds. Between 12 and 15 meters, the flood extent passes from 21% to 47% of the modelled domain, progressing essentially in the LA-domain. Above 21 m, most of the inner natural levees are below water and inundation expands almost the modelled domain.

Table 1. Results of horizontal accuracy for flood extent modelling

Water level	Comparison number	TS	BIAS
All	24	62	20
<12 m	1	24	-88
>12 m and <15 m	2	48	-19
>15 m and<21 m (rising water)	6	58	38
>15 m and<21 m (falling water)	4	65	22
>21 m	11	70	27

Velocity

Computed and simulated CC-velocities are in satisfactory agreement. The model correctly simulates the variation amplitude, with velocities values, ranging from -101.3 $cm.s^{-1}$ to 56.7 $cm.s^{-1}$. Over the whole simulated period, the correlation coefficient and NSE were superior to 0.83 and 0.68, respectively. The RMSE remained below 23.5 $cm.s^{-1}$. The outflow peaks can vary between -24 % (2009-2010) to +28 % (2014-2015). Conversely, inflow peaks remain similar with little inter-annual variations (SD=4.8 $cm.s^{-1}$).

B. Patterns of water circulation and flood duration

Seasonal patterns

The model simulated contrasted velocity magnitudes over the three domains, and high magnitude variation between hydrological periods (Figure 2). Regardless the hydrological period, the highest velocity magnitudes are encountered in CC-domain with values over 5.0 cm.s^{-1} at high water, and the lowest in LA-domain with a mean value inferior to 1.7 cm.s^{-1}. Velocity magnitudes exhibit little variations in SS-domain (0.8-1.7 cm.s^{-1}), while they range between 5.1 cm.s^{-1} during early low water (0.2 cm.s^{-1} at late low water) and 20.1 cm.s^{-1} (6.2 cm.s^{-1}) during high water in CC-domain (LA-domain). In SS-domain, the velocity magnitude is maximum during the falling period.

The water circulation patterns are highly variable along the HY. Until early rising water, CC-domain acts as an inlet. From late rising water to falling water, water circulation in the three domains is organized toward the mainstream. At early low water, the river flows into the LA- and SS-domain. Between early low water and early rising water, the rise of the local runoff counterbalances the increase of rivers-to-FP discharge, limits the river incursion into SS-domain and spreads over LA-domains. The moving frontier position between mainstream water and water coming from the local drainage watershed is well-defined, around the mid-course of SS-domain. During late rising water and high water, overflow induces a significant velocity magnitude increase in the north-eastern part of LA-domain and in CC-domain, and also a circular water circulation. At falling water, flows are organized towards the mainstream in all domains.

Water circulation results in contrasted inundation frequency across the FP (Figure 3). On average over the studied period, SS and CC-domains and the inner-channels in the LA-domain remain inundated all year-round. Some ponds located in the north-west of LA-domain, but also some located in the CC-domain also remain flooded all year-round. Inundation frequency is reduced by 20% (about 2 months and a half) in the flat LA-embayment and small bays along SS-domain. The inundation duration of levees and creeks is less than 6 months while some topographical features remain free of water all year-round, leaving some wetlands disconnected a large part of the HY.
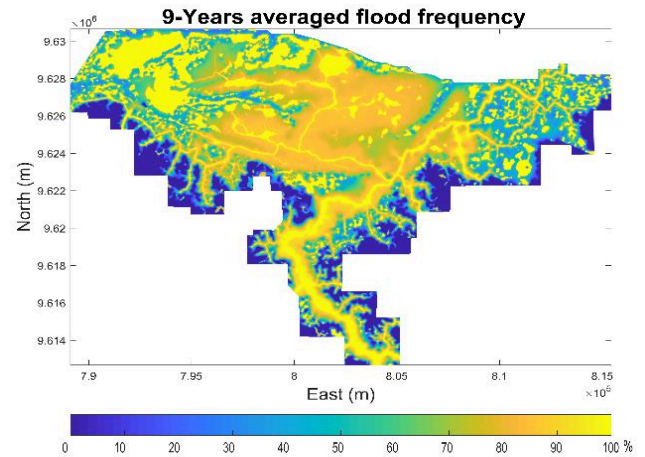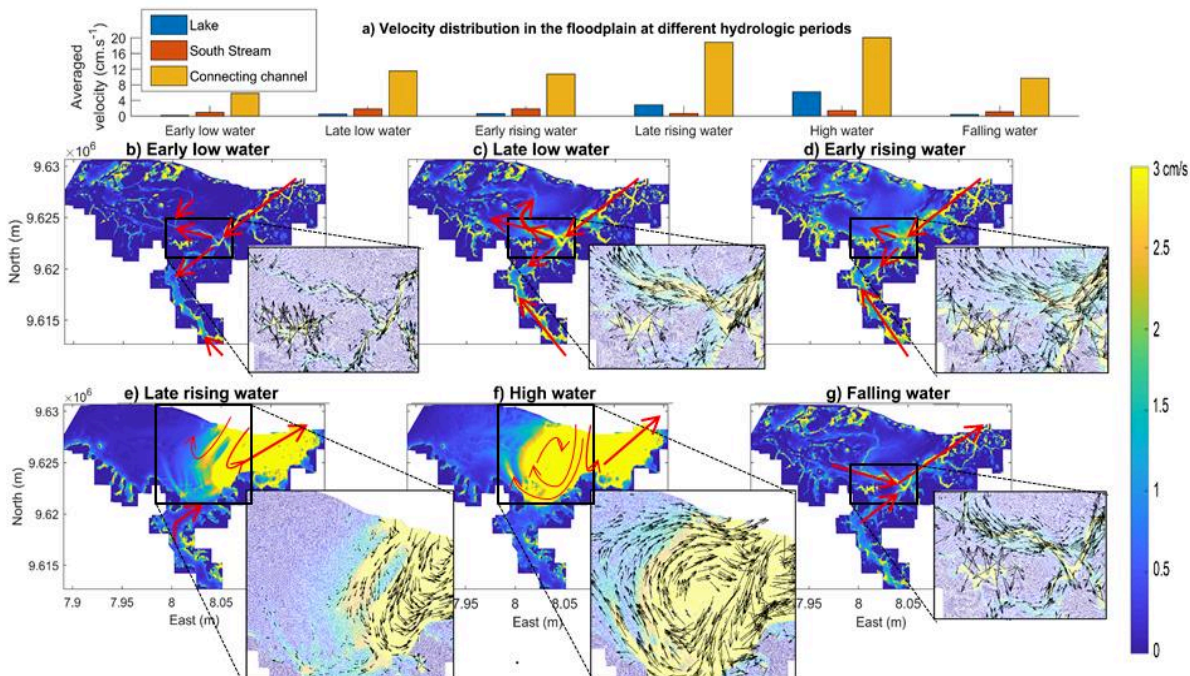

Figure 3. Nine-years averaged frequency flood map.

Figure 2. a) Average velocity distribution following the hydrologic period; b)-g) Velocity distribution in the FP at different hydrological periods with velocity magnitude in cm.s-1 set as background. The schematic red and black arrows indicate the direction of water circulation.

Extreme events impact upon flood duration

Extreme events influence the inundation duration across the FP (Figure 4a-e). Compared to normal hydrological year, the inundation duration during the 2009-2010 drought was reduced by more than a month in a large region of the LA-domain and in the small creeks and bays along the SS-domain (Figure 4a-b). Interestingly, extreme floods impact varies as a function of the considered event. As expected, extreme floods cause an increase of the inundation duration for pixels located along the margins of the different domains (LA, CC, SS), that are not inundated or only immerged a couple of months during a normal HY. For pixels in the LA-domain, which are usually flooded more than half a hydrological year, the inundation duration may reduce up to 20 days (e.g. during 2011-2012 Figure 4d) or increase up to 50 days (e.g. during 2014-2015 Figure 4e). In addition, in the CC and the central part of the SS domains, the inundation duration increases between 10 and 20 days as a function of the HY.

V. DISCUSSION

A. Model reliability

Model performances

Over the whole study period, the simulated water level and flood extent were in good agreement with the observations. However, both vertical and horizontal assessment underlined a degradation of accuracy during low water, as reported in other studies about Amazonian FP hydrodynamics [e.g. 19]. This deterioration is likely due to an under-representation of the inner-drainage channels that organize the flooding and the falling period [14]. Besides, the quality of the observation datasets should slightly lower during low water: i) the RL1 and RL2 could have remained out of water ii) the probability of mixed water-non water pixels increases. During high water, our analysis highlighted slight vertical and horizontal underestimation that we associate to little inaccuracies of bank elevations or locations for the WLBC, leading to slight overflow underestimation.

The model was able to simulate the CC-velocities variations. It also reproduces that the flow reversion in the channel and that overflow is the main water inflow pathway. However, the model delays the overflow onset of roughly 15 days, more likely because levee elevation is slightly overestimated. Levee overestimation also induces a slight overflow underestimation that is reflected in the computed velocities at high water.

Limitations and recommendations

The analysis of the model performance evidenced the topographic controls. Hence, modellers should take into account both the accuracy and the resolution of input topography. Here, ALOS-1/PALSAR images allowed detecting several channels whose width remains inferior to the minimum mesh edge size (23 m). In addition, forested wetlands present pronounced microtopography (hummocks and hollows) that affect the local water velocity field. With a 23m-mesh resolution, the model does not capture such fine-scale topographic controls. However, these features were taken into account through the roughness coefficient that is adjusted during the model calibration.

This study highlighted the necessity of controlling the quality of the validation datasets. Indeed, both observed water level and flood extent suffer from degradation at low water preventing robust validation at that period. Besides, simulated velocity fields cannot be fully (spatially and temporally)

HY	HY duration (days)	Initial WL (m)	Max. WL (m)	Final WL (m)	Ris. vel* (cm.day⁻¹)	Rec. vel** (cm.day⁻¹)
2007-2008	369	11.4	22.6	12.4	6.0	14.3
2009-2010	360	10.9	22.0	10.3	5.5	17.6
2008-2009	394	12.4	24.0	10.9	7.9	21.4
2011-2012	370	11.5	24.3	11.1	9.8	21.4
2014-2015	386	14.1	24.4	11.3	5.8	26.6

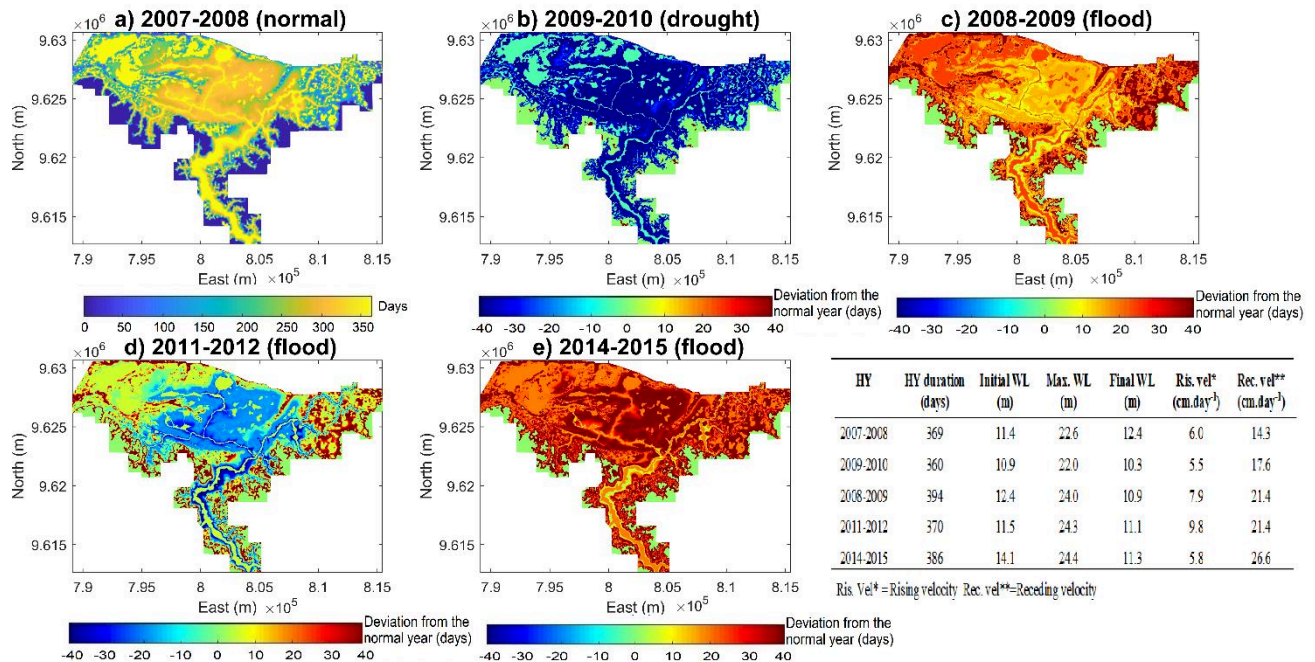Ris. Vel* =Rising velocity Rec. vel**=Receding velocity

Figure 4. a) Spatial distribution of inundation duration for a hydrological normal year, deviations from the normal year, b) a drought hydrological year, c-e) flood extreme events.
The table indicates the hydrological year characteristics (duration, min. and max)

validated with observations. Nevertheless, velocities validation indicates that CC-velocities are correctly estimated giving confidence for the other FP domains.

The presented model could have been more sophisticated by including the evolution of bottom shear stress or the wind effect. Unfortunately, no data upon vegetation growth were available for this study. Regarding the wind effect, Amaral et al. (2018) showed in the same floodplain that sites with more wind exposure have different biogeochemical characteristics than wind protected areas. Even if both variables may have impact on our results, the topography data remain the primary source of model uncertainty.

Despite these limitations, the good agreement between observed and simulated data suggests the hydrological-2D-hydrodynamics modelling is sufficient to capture the flow in the floodplain. Finally, our modelling approach only required a limited *in situ* data (bathymetry and velocity observation). Hence, our methodological framework can be transferred to any floodplain in the world.

B. Water circulation pattern: seasonal and spatial distribution

The seasonal and spatial velocity magnitude evolution and the distribution of inundation duration reported in this study reveal the complexity of water circulation patterns as already reported in [29] at regional scale and in [17,18] for a larger Amazon FP system. The inundation extent, duration and velocity magnitude in the different domains of the FP are only partly controlled by topography. As expected, current CC-velocities magnitude is significantly higher where the flow is well constrained by levees. Velocity magnitudes are also greater in SS-domain than in LA-domain, but not during late rising water and high water when overflow occurs in the north-westward region of LA-domain (Figure 4a-d). Our results suggest the importance of hydraulic controls.

During the early rising period (water level <17 m), water slopes in CC are positive and in opposite direction than those in SS and in a higher magnitude (0.6 cm.km^{-1} in CC against -6.82.10[-4] cm.km^{-1} in SS). The river incursion into the channel is limited by local runoff (maximum at this period) and spreads rather over the LA-domain. However, later in the rising period (17< water level <20 m), when local runoff already diminished, slopes equilibrate between these two domains allowing the river progression along SS. For water level higher than 20 m (high water and overflow period), there are no velocity magnitudes differences between rising and receding periods. This period also corresponds to maximum velocity in the LA-domain. At this period, flows have a circular pattern driven by topography and hydraulic controls exerted by SS-domain and the Amazon/Solimões River that act as hydraulic barriers. That the mainstream partly blocks the FP output is not surprising as such effect is already reported for Amazon River tributaries [30]. However, the role of local runoff upon river incursion is much less documented. Based on regional remote sensing analysis, [29] mentioned the role of FP water saturation prior to mainstream inundation as a main factor to explain the river incursion extent across the FP. During late high water and falling water, the main hydrodynamics driver

stays the Amazon/Solimões that keep on acting as a hydraulic barrier. The flood receding phase of the mainstream starts before ones of the Janauacá FP. Consequently, it induces a strong gradient between FP water level and mainstream stages (computed CC-slope of -5.4 cm.km^{-1}). This hydraulic gradient may also be the main driver of SS-velocity during falling water. During this period, LA-domain loses its direct connection with the mainstream (the mainstream margins) and velocity falls back to moderate velocity (< 2 cm.s^{-1}). Our findings support Alsdorf et al. (2007) statement upon the difficulty to retrieve water circulation from FP topography only. They also confirm those obtained by Ji et al, (2019) on another Amazonian FP that highlighted a strong interplay between local rainfall/runoff and river rising/receding rate.

C. Extreme events impact upon flood inundation

Based on our findings for the 2009-2010 drought, the inundation duration is reduced, especially in the LA-domain where the topography is relatively flat. Conversely, the study period encompasses three important floods events (2008-2009, 2011-2012, and 2014-2015). The flood amplitude obviously controls the inundation extent and thus controls the inundation duration of pixels with bottom elevation above the "normal" maximum flood amplitude. On the other hand, changes in inundation duration for pixels that are "normally" flooded differ between flood events, especially in the LA-domain. These differences reflect FP saturation conditions prior to inundation (i.e. the initial FP water volume) and the strength of the hydraulic control exerted by the Amazon/Solimões River, which vary inter-annually. At the beginning of the 2014-2015 cycle, the minimum stage was roughly 2 meters above that of 2008-2009 and 2.5 m above that of 2011-2012. We appraised the strength of hydraulic control by the Amazon/Solimões River though rising and receding water rates for water level ranging between 14 and 20 m (Figure 4). The rising rate was the highest during the 2011-2012 hydrological year, and the smallest during 2014-2015 hydrological year. The receding rate was the highest during the 2014-2015 hydrological year and was equal during the 2008-2009 and 2011-2012 hydrological years. Thus, the difference of positive inundation duration anomaly observed between 2014-2015 and 2008-2009 hydrological years might be explained by the prior inundation condition in 2014-2015. The negative inundation duration anomaly during 2011-2012 hydrological year should result from higher rising water rate while receding water rate is comparable to 2008-2009 hydrological year.

V.   CONCLUSION

Based on a hydrologic-2D hydrodynamic modelling (LUMP-FP and Telemac-2D), we investigate flooding dynamics across a medium-size Amazonian floodplain system (786 km[2], including the local catchment). The proposed approach integrates *in situ* data and remote sensing into a hydrologic-hydrodynamic model to simulate a 9-years period (2006-2015) that encompass floods and drought events. The model correctly reproduced water level, flood extent and velocity. However, its accuracy varies along the hydrological year. Indeed, misrepresentation of inner-channels and

imprecision in levee elevation slightly lower the accuracy of the model at low water period and high water, respectively.

The analysis of velocity spatiotemporal patterns highlights strong heterogeneities in water velocity magnitude between the different morphological domains of the floodplain. The river-floodplain connecting channel (CC-domain), where flow is well constrained by levees, presented the highest velocities, and the large embayment (LA-domain) in the northern-westward direction the lowest, except during high water. However, topography only partly controls the water circulation. Flows are also constrained by the interplay between mainstream and local runoff at least part of the hydrological year. Comparing several hydrological years highlights the interannual changes of these hydraulic controls in function of mainstream rising and receding rates, the local runoff and the influence exerted by prior inundation conditions.

Seasonally and spatially contrasted velocities across the FP imply spatially contrasted inundation duration. Drought essentially modifies SS-domain velocities, where higher values are encountered during the rising and late rising periods. It also reduces the velocity in the LA-domain during the high water, and consequently every mixing process in this area. The inundation duration is reduced, especially in the flat LA-domain. Flood events slightly affect the velocity magnitude at late rising water and high water (overbanking) and alter the duration of seasonal velocity patterns. While the flood amplitude controls the inundation extent, the rate of the rising/receding water in the mainstream and the prior inundation conditions control the inundation duration in the floodplain during flood events. Consequently, extreme flood amplitude does not necessary implies longer inundation duration. The latter results are also important while considering the potential impact of dams. Indeed, hundreds of spatially distributed dams across the Amazonian basin will not only affect the water level range in the dammed rivers but also the rising and receding rates of the associated rivers and far downstream with hardly foreseeable impacts.

The seasonal pattern of water circulation and inundation duration exhibits strong intra- and inter-annual variations. As these hydrodynamic features are key factors upon suspended solids transport, biogeochemical processes distribution, these parameters should be more cautiously taken into account in multi-disciplinary studies.

REFERENCES

[1]   Hess, L.; Melack, J.M.; Affonso, A.G.; Barbosa, C.; Gastil-Buhl, M.; Novo, E.M.L.M. "Wetlands of the Lowland Amazon Basin: Extent, Vegetative Cover, and Dual-season Inundated Area as Mapped with JERS-1 Synthetic Aperture Radar". *Wetlands* **2015**, *35*, 745–756.

[2]   Fassoni-Andrade, A.C.; Paiva, R.C.D. de "Mapping spatial-temporal sediment dynamics of river-floodplains in the Amazon". *Remote Sens. Environ.* **2019**, *221*, 94–107.

[3]   Moreira-Turcq, P.; Bonnet, M.P.; Amouroux, D.; Bernardes, M.C.; Lagane, C.; Maurice-Bourgoin, L.; Perez, M.; Seyler, P. "Seasonal variability in concentration, composition, age, and fluxes of particulate organic carbon exchanged between the floodplain and Amazon River". *Global Biogeochem. Cycles* **2013**, *27*, 119–130.

[4]   Barbosa, P.M.; Farjalla, V.F.; Melack, J.M.; Amaral, J.H.F.; da Silva, J.S.; Forsberg, B.R. "High rates of methane oxidation in an Amazon floodplain lake". *Biogeochemistry* **2018**, 351–365.

[5]   Richey, J.E.; Mertes, L.; Dunne, T.; Victoria, R.L.; Forsberg, B.R.; Tancredi, A.C.F.N.S.; Oliveira, E.; Victoria, R.L.; Forsberg, B.R.; Tancredi, A.C.F.N.S. "Sources and routing of the Amazon River flood wave". *Global Biogeochem. Cycles* **1989**, *3*, 191–204.

[6]   Castello, L.; Hess, L.; Thapa, R.; McGrath, D.G.; Arantes, C.C.; Renó, V.F.; Isaac, V.J. "Fishery yields vary with land cover on the Amazon River floodplain". *Fish Fish.* **2018**, *19*, 431–440.

[7]   Da Silva, V.; Trujillo, F.; Martin, A.; Zerbini, A.N.; Crespo, E.; Aliaga-Rossel, E.; Reeves, R. 2018.Inia geoffrensis. "The IUCN Red List of Threatened Species 2018" e.T10831A50358152. In; 2018.

[8]   Anderson, E.P.; Jenkins, C.N.; Heilpern, S.; Maldonado-Ocampo, J.A.; Carvajal-Vallejos, F.M.; Encalada, A.C.; Rivadeneira, J.F.; Hidalgo, M.; Cañas, C.M.; Ortega, H.; et al. "Fragmentation of Andes-to-Amazon connectivity by hydropower dams". *Sci. Adv.* **2018**, *4*, 1–8.

[9]   Castello, L.; Macedo, M.N. Large-scale degradation of Amazonian freshwater ecosystems. *Glob. Chang. Biol.* **2016**, *22*, 990–1007.

[10]   Gurnell, A.; Petts, G. Hydrology and Ecology of River Systems. In *Treatise on Water Science*; 2010; Vol. 2, pp. 237–269 ISBN 9780444531933.

[11]   Bonnet, M.P.; Pinel, S.; Garnier, J.; Bois, J.; Bonaventura, G.; Seyler, P. "Amazonian floodplain water balance based on hydrologic and electrical conductivity data analyses and modelling". **2017**, 1–38.

[12]   Bates, P.; De Roo, a. P.. "A simple raster-based model for flood inundation simulation". *J. Hydrol.* **2000**, *236*, 54–77.

[13]   Luo, X.; Li, H.Y.; Ruby Leung, L.; Tesfa, T.K.; Getirana, A.; Papa, F.; Hess, L. "Modeling surface water dynamics in the Amazon Basin using MOSART-Inundation v1.0: Impacts of geomorphological parameters and river flow representation". *Geosci. Model Dev.* **2017**, *10*, 1233–1259.

[14]   Wilson, M.D.; Bates, P.; Alsdorf, D.E.; Forsberg, B.R.; Horritt, M.S.; Melack, J.M.; Frappart, F.; Famiglietti, J. "Modeling large-scale inundation of Amazonian seasonally flooded wetlands". *Geophys. Res. Lett.* **2007**, *34*, L15404.

[15]   Frias, C.E.; Abad, J.D.; Mendoza, A.; Paredes, J.; Ortals, C.; Montoro, H. "Planform evolution of two anabranching structures in the Upper Peruvian Amazon River". *Water Resour. Res.* **2015**, *51*, 2742–2759.

[16]   Mendoza, A.; Abad, J.D.; Frias, C.E.; Ortals, C.; Paredes, J.; Montoro, H.; Vizcarra, J.; Simon, C.; Soto-Cortes, G. "Planform dynamics of the Iquitos anabranching structure in the Peruvian Upper Amazon River". *Earth Surf. Process. Landforms* **2016**, *41*, 961–970.

[17]   Rudorff, C.M.; Melack, J.M.; Bates, P. "Flooding dynamics on the lower Amazon floodplain: 2. Seasonal and interannual hydrological variability". *Water Resour. Res.* **2014**, *50*, 635–649.

[18]   Rudorff, C.M.; Melack, J.M.; Bates, P. "Flooding dynamics on the lower Amazon floodplain: 1. Hydraulic controls on water elevation, inundation extent, and river-floodplain discharge". *Water Resour. Res.* **2014**, *50*, 619–634.

[19]   Sioli, H. "The Amazon and its main afluents: Hydrography,

morphology of the river courses and river types". In *The Amazon Liminology and landscape ecology of a mighty tropical river and its basin*; 1984; pp. 127–165 ISBN 978-94-009-6544-7.

[20] Hervouet, J.M. "TELEMAC modelling system: an overview". *Hydrol. Process.* **2000**, *14*, 2209–2210.

[21] Lang, P.; Desombre, J.; Ata, R. TELEMAC-2D Software Release 7.0 User Manual 2014, 1–115.

[22] Trevethan, M.; Santos, R. V.; Ianniruberto, M.; Oliveira, M.; Martinelli, A.; Gualtieri, C. "Influence of tributary water chemistry on hydrodynamics and fish biogeography about the confluence of Negro and Solimões rivers", Brazil. *11º Simpósio Int. Eco-hidráulica (ISE 2016)* **2016**, 16.

[23] Canadian Hydraulics "Centre Blue Kenue". Available online: http://www.nrc-cnrc.gc.ca/eng/ibp/chc/software/kenue/bluekenue.html (accessed on Sep 1, 2018).

[24] Verron, J.; Sengenes, P.; Lambin, J.; Noubel, J.; Steunou, N.; Guillot, A.; Picot, N.; Coutin-Faye, S.; Sharma, J.R.; Gairola, R.M.; et al. "The SARAL/AltiKa Altimetry Satellite Mission". *Mar. Geod.* **2015**, 00–00.

[25] Chapron, B.; McDonald, K.; Shimada, M.; Rosen, P. a.; Schroeder, R.; Hess, L. "Mapping Regional Inundation with Spaceborne L-Band SAR". *Remote Sens.* **2015**, *7*, 5440–5470.

[26] Arcement Jr, G.J.; Schneider, V.R. "Guide for Selecting Manning's Roughness Coefficients for Natural Channels and FloodPlains". *Tech. Report, Geol. Surv. Water-Supply, United States Gov. Print. Off. Washington, U.S.A* **1989**, 38.

[27] Pinel, S.; Bonnet, M.P.; Santos, J.; Moreira, D.; Calmant, S.; Satge, F.; Seyler, F. "Correction of interferometric and vegetation biases in the SRTMGL1 spaceborne DEM with hydrological conditioning towards improved hydrodynamics modeling in the Amazon basin". *Remote Sens.* **2015**, 16108–16130.

[28] Hutchinson, M.F. ANUDEM VERSION 5.3 USER GUIDE 2011.

[29] Mertes, L. "Documentation and significance of the perirheic zone on inundated floodplains". *Water Resour. Res.* **1997**, *33*, 1749.

[30] Paiva, R.C.D.; Buarque, D.C.; Collischonn, W.; Bonnet, M.P.; Frappart, F.; Calmant, S.; Bulhões Mendes, C.A. "Large-scale hydrologic and hydrodynamic modeling of the Amazon River basin". *Water Resour. Res.* **2013**, *49*, 1226–1243.